

Fault healing promotes high-frequency earthquakes in laboratory experiments and on natural faults

Gregory C. McLaskey¹†, Amanda M. Thomas², Steven D. Glaser¹ & Robert M. Nadeau²

Faults strengthen or heal with time in stationary contact^{1,2}, and this healing may be an essential ingredient for the generation of earthquakes^{1–3}. In the laboratory, healing is thought to be the result of thermally activated mechanisms that weld together micrometre-sized asperity contacts on the fault surface, but the relationship between laboratory measures of fault healing and the seismically observable properties of earthquakes is at present not well defined. Here we report on laboratory experiments and seismological observations that show how the spectral properties of earthquakes vary as a function of fault healing time. In the laboratory, we find that increased healing causes a disproportionately large amount of high-frequency seismic radiation to be produced during fault rupture. We observe a similar connection between earthquake spectra and recurrence time for repeating earthquake sequences on natural faults. Healing rates depend on pressure, temperature⁴ and mineralogy¹, so the connection between seismicity and healing may help to explain recent observations of large megathrust earthquakes which indicate that energetic, high-frequency seismic radiation originates from locations that are distinct from the geodetically inferred locations of large-amplitude fault slip^{5–7}.

In laboratory measurements, static-fault frictional strength, μ_s , is generally observed to increase linearly with the logarithm of time in stationary contact, t_{hold} , according to

$$\mu_s(t_{\text{hold}}) = \alpha_s + \beta_s \log_{10}(t_{\text{hold}}) \quad (1)$$

where β_s is the healing rate and α_s is the fault strength at time $t_{\text{hold}} = 1$ s (refs 1–4, 8). These measurements are used to derive rate- and state-dependent friction laws^{2,3} that have provided insight into fault behaviour ranging from slow slip to dynamic rupture^{2,8–10}. Healing rates have also been inferred from repeating earthquake sequences^{10–12} (RESs). These are sets of events with nearly identical waveforms, locations and magnitudes, and are thought to represent the repeated rupture of a patch of fault that is slowly loaded by aseismic slip of the surrounding material. Here we consider the stick-slip behaviour of a laboratory fault as a proxy for such a fault patch and compare our results with observations of RESs on the San Andreas fault. In addition to measuring static friction, slip and stress drop, we record the stress waves emitted during the rupture of the laboratory fault, which we call laboratory earthquakes (LabEQs). This facilitates a link between friction properties observed in the laboratory and earthquakes produced on natural faults.

Fault healing is typically attributed to an increase in either the area or the strength of asperity contacts due to ‘creep’^{2,3}. Mechanisms may include stress-induced diffusion, dislocation motion, chemically aided slow crack growth, dissolution–precipitation processes and other thermally activated processes^{2,3,13–15}. Although specific mechanisms may differ, the overall effects of healing are remarkably similar. Equation (1) is applicable to rocks¹, metals¹⁶, plastics⁴ and paper¹⁷, which suggests that the mechanics of healing are not greatly dependent on specific chemical or physical properties, but rely on universally observed

surface properties such as multiscale roughness. A better understanding of the relationship between fault healing and earthquake generation may be the key to understanding the physics of earthquakes¹⁸.

We use test blocks composed of the glassy polymer poly(methyl methacrylate) (PMMA). This and similar glassy polymers are commonly used as model materials for fault rupture and friction studies^{2,4,19,20}. Friction on PMMA–PMMA interfaces obeys equation (1) and is well modelled by the rate- and state-dependent friction laws^{2,4}. Because of PMMA’s low hardness and melting temperature (~ 160 °C), the behaviour of PMMA–PMMA interfaces at room temperature and modest stress levels (100 kPa) may be somewhat representative of the behaviour of rocks at depth²⁰. The similarities and differences between plastic and rock may serve as important points of comparison when studying the range of friction properties expected in the brittle–ductile spectrum of crustal deformation behaviour.

Stick-slip experiments are conducted at room temperature (20 °C) and humidity (30% relative humidity) on a direct-shear apparatus consisting of a PMMA slider block (181 mm long, 60 mm wide, 17 mm high) and a larger PMMA base plate (450 mm long, 300 mm wide, 36 mm high) (Fig. 1a, inset). With the normal force, F_N , held constant, the shear force, F_S , is increased until the sample undergoes a series of stick-slip instabilities, denoted events. The recurrence time, t_r , defined as the time since the previous event, is computed for each pair of consecutive events in the sequence. (Despite subtle differences between them²¹, we assume that $t_r = t_{\text{hold}}$.) Each event produces a LabEQ, which is recorded with piezoelectric sensors attached to the PMMA base plate. The slider block slips 50–200 μm during each event. Some slow premonitory slip (~ 2 μm) is often detected 1–2 ms before rapid slip commences. We detect no slip between events (to the ~ 1 - μm noise level). The duration of slip for each event is approximately constant (8 ms) and is probably controlled by the combined stiffness of the apparatus and samples rather than fault rupture properties.

Load point displacement, x_{LP} , is controlled by turning a fine-threaded screw that presses against the trailing edge of the slider block. When the load point velocity, $v_{\text{LP}} = dx_{\text{LP}}/dt$, is systematically increased or decreased, large variations in t_r can be achieved in a single experimental run, while other experimental variables (F_N , surface conditions and so on) are kept constant. Typical results are shown in Fig. 1. To isolate cumulative wear and loading-rate effects, experimental runs were conducted in pairs: one with increasing v_{LP} (Fig. 1a) and one with decreasing v_{LP} (Fig. 1b). For every event in each stick-slip sequence, we measure F_{max} and F_{min} (Fig. 1) and calculate the stress drop $\Delta\tau = (F_{\text{max}} - F_{\text{min}})/A$, where A is the nominal fault area (0.0109 m²). These parameters are plotted against $\log_{10}(t_r)$ (Fig. 1b, inset, and Supplementary Figs 2–4). Slopes, β , and intercepts, α , of the best-fit lines are reported in Supplementary Table 1. All tests show results consistent with equation (1) and previous work^{13,4,8}. The increase in $\Delta\tau$ with increasing t_r is due to both an increase in F_{max} and a decrease in F_{min} with $\log_{10}(t_r)$ (refs 8, 21). In all cases, healing rates, β , are slightly larger for runs with decreasing v_{LP} than for runs with increasing v_{LP} , indicating a dependence on loading rate or stress time history.

¹Department of Civil and Environmental Engineering, University of California, Berkeley, California 94720, USA. ²Department of Earth and Planetary Science, Berkeley Seismological Laboratory, University of California, Berkeley, California 94720, USA. †Present address: United States Geological Survey, 345 Middlefield Road, MS 977, Menlo Park, California 94025, USA.

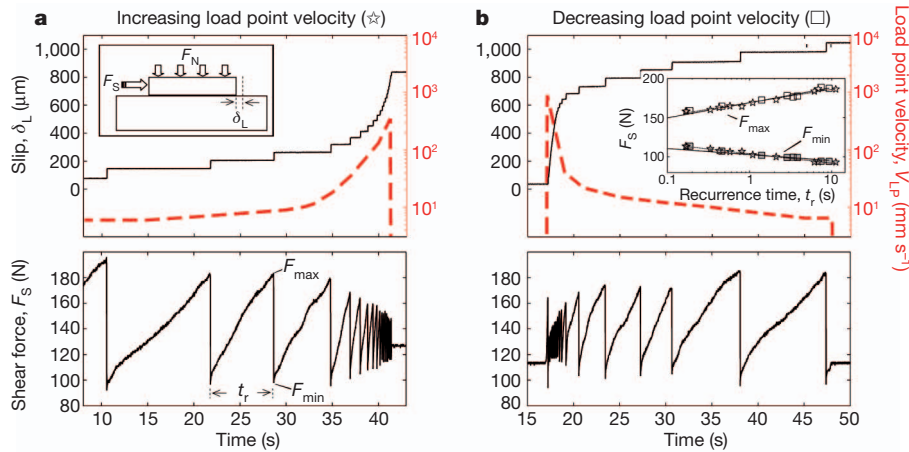


Figure 1 | Experimental data from a pair of healing tests. Shear force, F_S , load point velocity, v_{LP} (dashed line), and slip δ_L , measured from stick-slip experiments at $\sigma_n = 36$ kPa. All experiments were conducted in pairs, one with increasing v_{LP} (**a**) and one with decreasing v_{LP} (**b**). Insets: schematic of the

apparatus (**a**) and the maximum (F_{max}) and minimum (F_{min}) shear forces measured for each event in the stick-slip sequence and plotted against the logarithm of t_r (**b**). Stars and squares are from runs with increasing and decreasing v_{LP} , respectively.

An example sequence of LabEQ seismograms is shown in Fig. 2. The interface properties, apparatus and specimen stiffness, sensor response and wave propagation characteristics do not change between successive events, so differences between LabEQs are attributed to variations in t_r . When each seismogram is scaled with respect to the total measured slip, δ_β , the low-frequency components (Fig. 2a) are nearly identical but the high-frequency components (Fig. 2b) depend strongly on

t_r . Absolute source spectra were estimated for each LabEQ by removing the instrument and apparatus response functions from recorded signals by means of a ball-drop calibration source (Methods). Examples of absolute source displacement spectra are shown in Fig. 3a for three LabEQs from Fig. 2. Each source spectrum is roughly linear in $\log(\omega)$, where ω is the angular frequency, so spectra were fitted with best-fit lines (not shown). Variations in the spectral slopes

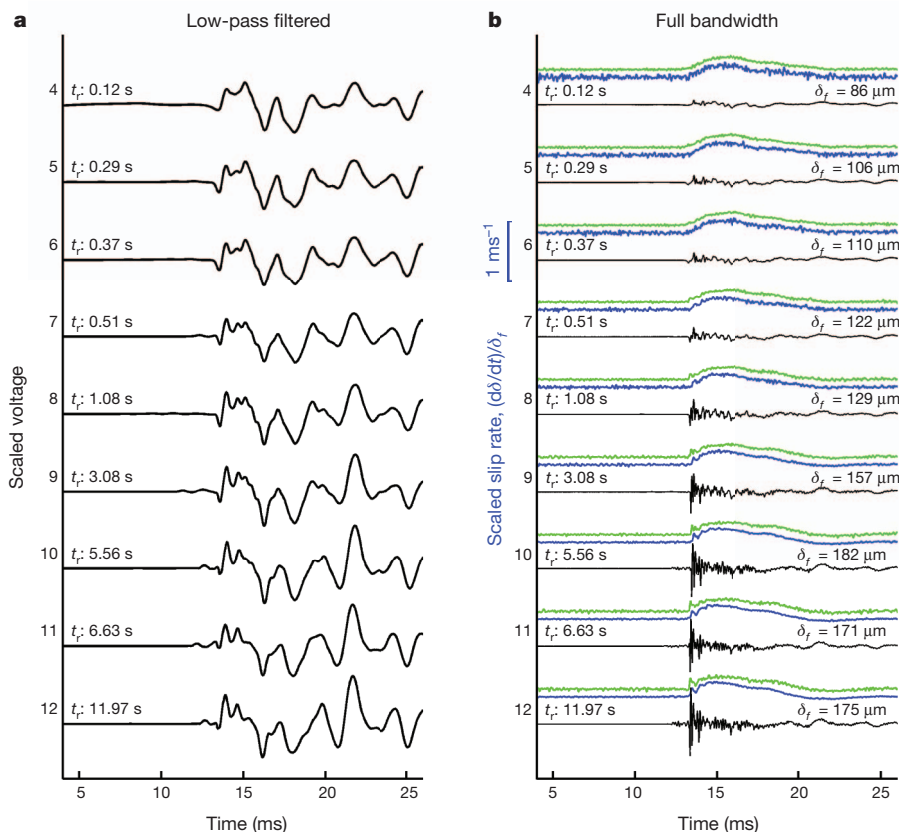


Figure 2 | Sequence of successive LabEQs. Events from an experimental run with decreasing v_{LP} (increasing time between successive events) at $\sigma_n = 130$ kPa and using a rough sample (run 45-R-Dec; see Supplementary Table 1). Each trace is scaled by the total measured slip, δ_β indicated for each trace. **a**, Low-pass-filtered signals (1-kHz cut-off) illustrating the similarity of

low-frequency waveforms. **b**, Full-bandwidth recorded LabEQ data (raw sensor output) plotted alongside scaled slip rates $(d\delta/dt)/\delta_\beta$ which are derived from slip measured at the leading (blue) and trailing (green) edges of the slider block and low-pass-filtered at 5 kHz to reduce high-frequency noise. The green curves have the same scale as the blue curves, and are offset for clarity.

of LabEQ source spectra are shown in Fig. 3b for all 46 events from four tests conducted at normal stress, $\sigma_n = 130$ kPa. These laboratory results show a disproportionate increase in high-frequency ground motions for greater t_r . Similar spectral changes were observed for all experiments, but are most pronounced for those conducted at higher σ_n . Peak high-frequency ground motions coincide with the initiation of slip, not maximum slip rate.

To complement the laboratory results, we analysed RESs on the San Andreas fault^{22,23} that were perturbed by the 2004, moment-magnitude $M_w = 6$ Parkfield, California earthquake. As shown in Fig. 4, an increase in high frequencies with increasing t_r was observed for most RESs. Similar trends were found for the CA1 RES on the Calaveras fault¹¹. If spectral changes were due to a propagation effect, such as damage from the Parkfield earthquake, we would expect the effects to be more pronounced in recordings from source–station ray paths that traverse long distances through zones of expected damage²⁴ (that is, near or within the fault zone and at shallower depths) (Supplementary Fig. 6 and Supplementary Table 2). Instead, many stations see similar spectral variations between the same events and spectral changes vary among RESs (Supplementary Fig. 1), so we suspect that spectral variations are dominantly controlled by changes in earthquake source characteristics and not path effects.

Fault healing seems to cause spectral changes over a broad range of frequencies (Fig. 3a), so we propose that our observations are applicable

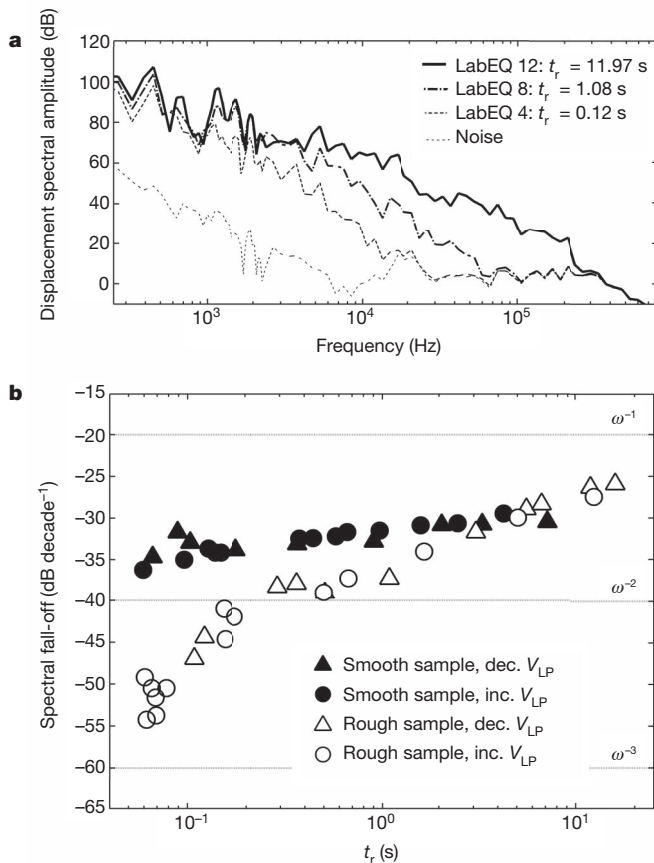


Figure 3 | LabEQ spectral changes with recurrence time. **a**, Source displacement spectra and the noise spectrum from three of the LabEQs shown in Fig. 2, which span two orders of magnitude in t_r . **b**, Slope of source spectrum as a function of recurrence time for all LabEQs from four experimental runs conducted at $\sigma_n = 130$ kPa. Only the frequency band with a signal-to-noise ratio greater than 6 dB was used for the calculation of these spectral slopes. For the rough sample, spectral slopes increase from $\omega^{-2.5}$ to $\omega^{-1.5}$ with increasing t_r . LabEQs generated from the smooth sample show subtle but systematic spectral changes.

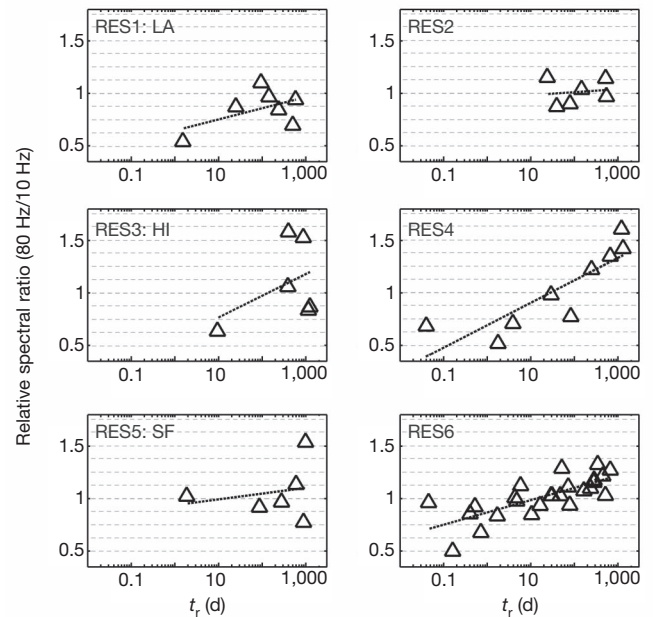


Figure 4 | Spectral changes of RESs near Parkfield. The SF, LA and HI RESs were targeted for penetration by the SAFOD deep-drilling experiment (sequences NW, SE and S1 in ref. 23). Relative spectral ratios are calculated from the ratio of relative spectral amplitudes at 75–85 Hz to those at 5–15 Hz (Supplementary Fig. 5 and Supplementary Table 3). Data points indicate the averages of the relative spectral ratios obtained from ground motions recorded at at least three stations for each event in each RES. Dotted lines show a linear best fit to the data, and a positive slope indicates increasing high-frequency ground motions (relative to low-frequency ground motion) with increasing $\log_{10}(t_r)$.

not just to the small length scales and high frequencies of LabEQs, but to natural faults and great earthquakes as well. To discuss the underlying mechanisms of these spectral changes, we present a conceptual fault model in which both natural faults and those in the laboratory are composed of a large number of asperity contacts^{2,25,26} with a distribution of strengths, which collectively sum to produce the static fault strength, μ_s . If the thermally activated healing mechanisms described above cause asperity contacts to strengthen at a rate proportional to the forces they support, then healing would promote a more heterogeneous spatial distribution of fault strength on the asperity scale. When this healed fault ruptures, its heterogeneous fault strength could cause perturbations in slip velocity that would generate high-frequency seismic waves²⁷. Alternatively, if healing promotes a larger stress drop^{8,21} or a more abrupt slip weakening behaviour, this would promote faster rupture propagation, which could also account for the enhanced high frequencies. This interpretation is consistent with a previous proposal that spectral changes observed for the CA1 RES signify shorter source duration, which could be explained by faster rupture propagation¹¹.

The spectral changes shown in Fig. 3b are somewhat analogous to those in Fig. 4, but when comparing the spectra of LabEQs with those from RESs, differences in rise time (the time during which a single point on the fault slips seismically) and rupture duration relative to the recorded frequency band should be taken into account. The LabEQ spectra shown in Fig. 3 are probably controlled by details of rupture propagation. Although the sample geometry and the resolution of the slip sensors do not permit a detailed analysis of dynamic rupture, Fig. 2b does show that slip accelerated more rapidly for events that healed longer. In the case of RESs, even the highest frequencies available for analysis (75–85 Hz) may be too low to contain much information about rupture propagation. Additionally, complicated interaction between rapid, unstable failure of the fault patch and stable slip imposed by slow slip of the surrounding region^{9,10} may contribute to

added differences between RESs at Parkfield and current laboratory analogues.

Dense seismic arrays have facilitated back-projection studies of recent megathrust earthquakes that highlight the temporal and spatial complexity of high-frequency seismic radiation and show that sources of high-frequency seismic waves are not spatially correlated with locations of maximum inferred fault slip^{5–7}. A mechanism related to fault healing may be responsible for these puzzling observations, particularly for the March 2011 Tohoku earthquake, where high frequencies originated from deeper sections of the fault and contributed to strong ground accelerations felt in eastern Japan. Laboratory experiments on glassy polymers show that healing rate, β_s , increases by an order of magnitude when temperature is increased to close to the glass transition⁴, so it seems possible that variations in healing rate—due to high pressures and temperatures or fault chemistry—could affect fault properties more profoundly than variations in recurrence time. If deeper sections of the fault are more healed than shallower fault sections, this might cause those parts to radiate more high-frequency energy when ruptured in a large earthquake.

The healing-related spectral changes observed in this study demonstrate how earthquake spectra are determined not simply by static fault strength or total fault slip, but by the manner in which slip occurs. Fault sections that heal rapidly or faults that heal for a long time, such as those associated with intraplate earthquakes in low-strain-rate environments, will produce higher-frequency earthquakes. In contrast, fault sections composed of materials that do not heal, such as smectite, a clay mineral found in the creeping section of the San Andreas fault²⁸ and in subduction zones²⁹, will slip slowly and smoothly.

METHODS SUMMARY

Sliding surfaces of laboratory specimens were milled flat and then roughened by hand lapping with either #60 grit or #600 grit abrasive, producing surface roughnesses referred to as rough and smooth, respectively. Shear force, F_s , was measured with a load cell located between the loading screw and the slider block. Fault slip, δ , was measured at both the leading edge (δ_l) and the trailing edge (δ_t) of the slider using eddy current sensors mounted on the samples. The loading screw was turned by hand; consequently, v_{LP} was not precisely controlled but was calculated from δ_t , F_s and the apparatus and specimen stiffness, which was constant for each run. Power spectral estimates were obtained by Fourier-transforming a 65.5-ms (laboratory) or 3.5–4-s (field) signal centred on the first arrival and tapered with a Blackman–Harris window. Noise spectra were obtained similarly. Only data with signal-to-noise ratio of at least 6 dB was used. LabEQs were recorded with a Panametrics V103 sensor located 80 mm from the laboratory fault. RESs near Parkfield were recorded as 250-Hz velocity seismograms by the borehole High-Resolution Seismic Network. Only vertical-component records were used for this study. RES detections and locations follow ref. 22. For each station and each RES, station averages were calculated by linearly averaging spectra from events cleanly recorded by all stations. We computed relative spectral amplitudes by dividing spectra of individual recordings by the station average. Relative spectral ratios were obtained from the ratio of relative spectral amplitudes at high frequencies (75–85 Hz) to those at lower frequencies (5–15 Hz). A different choice of high-frequency band (for example 65–75 Hz) does not affect the results.

Full Methods and any associated references are available in the online version of the paper.

Received 25 April; accepted 14 August 2012.

- Dieterich, J. H. Time-dependent friction in rocks. *J. Geophys. Res.* **77**, 3690–3697 (1972).
- Dieterich, J. H. & Kilgore, B. D. Direct observations of frictional contacts—new insights for state-dependent properties. *Pure Appl. Geophys.* **143**, 283–302 (1994).
- Scholz, C. *The Mechanics of Earthquakes and Faulting* 81–100 (Cambridge Univ. Press, 2002).

- Berthoud, P. & Baumberger, T. G'Sell, C. & Hiver, J.-M. Physical analysis of the state- and rate-dependent friction law: static friction. *Phys. Rev. B* **59**, 14313–14327 (1999).
- Kiser, E. & Ishii, M. The 2010 Mw 8.8 Chile earthquake: Triggering on multiple segments and frequency-dependent rupture behavior. *Geophys. Res. Lett.* **38**, L07301 (2011).
- Lay, T. *et al.* Depth-varying rupture properties of subduction zone megathrust faults. *J. Geophys. Res.* **117**, B04311 (2012).
- Meng, L., Inbal, A. & Ampuero, J.-P. A window into the complexity of the dynamic rupture of the 2011 Mw 9 Tohoku-Oki earthquake. *Geophys. Res. Lett.* **38**, L00G07 (2011).
- Karner, S. L. & Marone, C. in *Geocomplexity and the Physics of Earthquakes* (eds Rundle, J. B., Turcotte, D. and Klein, W.) 187–198 (Geophys. Monogr. Ser. 120, AGU, 2000).
- Chen, T. & Lapusta, N. Scaling of small repeating earthquakes explained by interaction of seismic and aseismic slip in a rate and state fault model. *J. Geophys. Res.* **114**, B01311 (2009).
- Chen, K. H., Bürgmann, R., Nadeau, R. M., Chen, T. & Lapusta, N. Postseismic variations in seismic moment and recurrence interval of repeating earthquakes. *Earth Planet. Sci. Lett.* **299**, 118–125 (2010).
- Vidale, J. E., Ellsworth, W. L., Cole, A. & Marone, C. Variations in rupture process with recurrence interval in a repeated small earthquake. *Nature* **368**, 624–626 (1994).
- Peng, Z. & Vidale, J. E. Marone, C. & Rubin, A. Systematic variations in recurrence interval and moment of repeating aftershocks. *Geophys. Res. Lett.* **32**, L15301 (2005).
- Dieterich, J. H. & Conrad, G. Effect of humidity on time and velocity-dependent friction in rocks. *J. Geophys. Res.* **89**, 4196–4202 (1984).
- Cox, S. F. & Paterson, M. S. Experimental dissolution precipitation creep in quartz aggregates at high temperatures. *Geophys. Res. Lett.* **18**, 1401–1404 (1991).
- Li, Q., Tullis, T. E., Goldsby, D. & Carpick, R. W. Frictional ageing from interfacial bonding and the origins of rate and state friction. *Nature* **480**, 233–236 (2011).
- Rabinowitz, E. *Friction and Wear of Materials* (Wiley, 1965).
- Heslot, F., Baumberger, T., Perrin, B., Caroli, B. & Caroli, C. Creep, stick-slip, and dry friction dynamics: experiments and a heuristic model. *Phys. Rev. E* **49**, 4973–4988 (1994).
- Rice, J. R. & Cocco, M. in *Tectonic Faults: Agents of Change on a Dynamic Earth* (eds Handy, M. R., Hirth, G. & Hovius, N.) 99–137 (MIT Press, 2007).
- Wu, F. T., Thomson, K. C. & Kuenzler, H. Stick-slip propagation velocity and seismic source mechanism. *Bull. Seismol. Soc. Am.* **62**, 1621–1628 (1972).
- McLaskey, G. C. & Glaser, S. D. Micromechanics of asperity rupture during laboratory stick slip experiments. *Geophys. Res. Lett.* **38**, L12302 (2011).
- Beeler, N. M., Hickman, S. H. & Wong, T.-f. Earthquake stress drop and laboratory-inferred interseismic strength recovery. *J. Geophys. Res.* **106**, 30,701–30,713 (2001).
- Nadeau, R. M. & McEvilly, T. V. Fault slip rates at depth from recurrence intervals of repeating microearthquakes. *Science* **285**, 718–721 (1999).
- Nadeau, R. M., Michalini, A., Uhrhammer, R. A., Dolenc, D. & McEvilly, T. V. Detailed kinematics, structure and recurrence of micro-seismicity in the SAFOD target region. *Geophys. Res. Lett.* **31**, L12S08 (2004).
- Rubinstein, J. L. & Beroza, G. C. Depth constraints on nonlinear strong ground motion. *Geophys. Res. Lett.* **32**, L14313 (2005).
- Johnson, L. An earthquake model with interacting asperities. *Geophys. J. Int.* **182**, 1339–1373 (2010).
- Dreger, D., Nadeau, R. M. & Chung, A. Repeating earthquake finite source models: strong asperities revealed on the San Andreas fault. *Geophys. Res. Lett.* **34**, L23302 (2007).
- Page, M., Dunham, E. & Carlson, J. M. Distinguishing barriers and asperities in near-source ground motion. *J. Geophys. Res.* **110**, B11302 (2005).
- Carpenter, B. M., Marone, C. & Saffer, D. M. Weakness of the San Andreas fault revealed by samples from the active fault zone. *Nature Geosci.* **4**, 251–254 (2011).
- Saffer, D. M. & Marone, C. Comparison of smectite- and illite rich gouge frictional properties: application to the updip limit of the seismogenic zone along subduction megathrusts. *Earth Planet. Sci. Lett.* **215**, 219–235 (2003).

Supplementary Information is available in the online version of the paper.

Acknowledgements This paper was improved by suggestions from R. Bürgmann and constructive reviews by T. Tullis, C. Marone, W. Ellsworth and N. Beeler. High-Resolution Seismic Network data was provided by the Berkeley Seismological Laboratory and NCEDC. Research was supported by the US NSF GRF and NSF grants CMMI-1131582, EAR-0738342 and EAR-0910322. This is BSL contribution #11-12.

Author Contributions G.C.M. and S.D.G. developed the laboratory experiments. R.M.N. developed and maintained repeating-earthquake catalogues. A.M.T. and G.C.M. performed analysis of the RESs at Parkfield. G.C.M. performed analysis of LabEQs and wrote the manuscript, with contributions from all authors.

Author Information Reprints and permissions information is available at www.nature.com/reprints. The authors declare no competing financial interests. Readers are welcome to comment on the online version of the paper. Correspondence and requests for materials should be addressed to G.C.M. (gmclaskey@usgs.gov).

METHODS

Laboratory. Fault slip, δ , is measured at both the leading edge (δ_L) and the trailing edge (δ_T) of the slider block using eddy current sensors mounted on the samples. The shear force, F_S , is measured with a load cell located between the loading screw and the slider block. The loading screw is turned by hand. Consequently, v_{LP} is not precisely controlled but is calculated from δ_T , F_S and the apparatus and specimen stiffness, which was constant for each run. Hydraulic cylinders apply F_N . Sliding surfaces were milled flat and then roughened by hand lapping with either #60 grit or #600 grit abrasive, producing surface roughnesses referred to as rough and smooth, respectively. F_S , δ_L and δ_T are recorded at 2 kHz throughout the experiment. A second system records LabEQs, F_S , δ_L and δ_T at 2 MHz for 262 ms around each event or set of events.

Spectral analysis. Power spectral estimates (PSEs) were obtained by Fourier-transforming a 65.5-ms (laboratory) or 3.5–4-s (field) signal centred on the first arrival and tapered with a Blackman–Harris window. Noise spectra were obtained similarly from signals recorded before the first arrival (field) or before the first event in each sequence (laboratory). Only data with a signal-to-noise ratio of at least 6 dB was used. LabEQs were recorded with a Panametrics V103 sensor

located 80 mm from the laboratory fault, and absolute source spectra were obtained by dividing PSEs by the PSE of a ball-drop calibration source (the stress waves due to a tiny ball impacting the base plate), which has a known source spectrum³⁰. Variations in spectra from ball-drop sources at different locations on the specimen indicate that absolute source spectra of LabEQs are accurate to ± 8 dB, and the precision is better than ± 2 dB. RESs near Parkfield were recorded as 250-Hz velocity seismograms by the borehole High-Resolution Seismic Network. Only vertical-component records were used for this study. RES detections and locations follow ref. 22. For each station and each RES, station averages were calculated by linearly averaging spectra from events cleanly recorded by all stations. We computed relative spectral amplitudes by dividing spectra of individual recordings by the station average. Relative spectral ratios were obtained from the ratio of relative spectral amplitudes at high frequencies (75–85 Hz) to those at lower frequencies (5–15 Hz). A different choice of high-frequency band (for example 65–75 Hz) does not affect the results.

30. McLaskey, G. C. & Glaser, S. D. Hertzian impact: experimental study of the force pulse and resulting stress waves. *J. Acoust. Soc. Am.* **128**, 1087–1096 (2010).